Exploring the many-body dynamics near a conical intersection with trapped Rydberg ions

Filippo M. Gambetta,[1, 2] Chi Zhang,[3] Markus Hennrich,[3] Igor Lesanovsky,[1, 2, 4] and Weibin Li[1, 2]

[1]*School of Physics and Astronomy, University of Nottingham, Nottingham, NG7 2RD, United Kingdom*
[2]*Centre for the Mathematics and Theoretical Physics of Quantum Non-equilibrium Systems,*
University of Nottingham, Nottingham NG7 2RD, United Kingdom
[3]*Department of Physics, Stockholm University, 10691 Stockholm, Sweden*
[4]*Institut für Theoretische Physik, University of Tübingen, 72076 Tübingen, Germany*
(Dated: December 4, 2020)

Conical intersections between electronic potential energy surfaces are paradigmatic for the study of non-adiabatic processes in the excited states of large molecules. However, since the corresponding dynamics occurs on a femtosecond timescale, their investigation remains challenging and requires ultrafast spectroscopy techniques. We demonstrate that trapped Rydberg ions are a platform to engineer conical intersections and to simulate their ensuing dynamics on larger length and time scales of the order of nanometers and microseconds, respectively; all this in a highly controllable system. Here, the shape of the potential energy surfaces and the position of the conical intersection can be tuned thanks to the interplay between the high polarizability and the strong dipolar exchange interactions of Rydberg ions. We study how the presence of a conical intersection affects both the nuclear and electronic dynamics demonstrating, in particular, how it results in the inhibition of the nuclear motion. These effects can be monitored in real time via a direct spectroscopic measurement of the electronic populations in a state-of-the-art experimental setup.

Introduction.— The Born-Oppenheimer (BO) approximation is a cornerstone of modern solid state and molecular theories [1, 2]. It provides a simple description of many electronic systems in which nuclei move on a single potential energy surface (PES) generated by the electronic dynamics. Nevertheless, non-adiabatic phenomena, which fall outside the validity regime of the BO approximation, are ubiquitous in many fundamental chemical processes [3]. Among them, conical intersections (CIs), which occur when two (or more) PESs are degenerate within a given sub-manifold of the nuclear coordinates, are at basis of many fundamental photo-chemical processes in large molecules [2, 4, 5]. They provide a fast and radiationless de-excitation mechanism between intra-molecular electronic states [6, 7], which contributes to the stability of DNA [8], to the mechanism of vision [9–11], and to photosynthesis [12]. Importantly, CIs are tightly linked to the emergence of geometric phase (GP) effects: during the motion on a path that encircles a CI, both the electronic and nuclear wavefunctions acquire an extra phase factor of π, which results in observable interference phenomena [13–19]. In the last decade a number of theoretical and computational tools confirmed the existence of CIs and their importance in photo-chemical reactions [2, 5, 20], though their experimental observation remains rather elusive. Indeed, since processes in which they are involved occur typically on a femtosecond timescale, ultrafast and broadband spectroscopy techniques are required to detect them directly [21–24]. In recent years, ultracold gases have been proposed as a tool to study CIs in the laboratory [25–27], with Rydberg atoms [28, 29] suggested as a quantum simulator for the dynamics in the neighborhood of a CI [30, 31].

In this work we show that trapped Rydberg ions offer ideal properties for controlling and investigating the quantum many-body dynamics near a CI. They combine the high degree of control typical of trapped ion setups with tunable dipole-dipole interactions, enabled by the possibility to individually excite
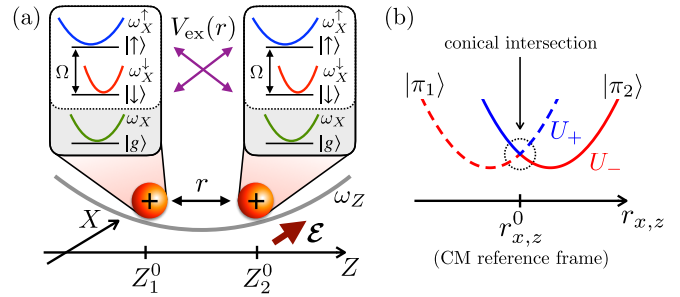
FIG. 1. **Conical intersection in a system of two Rydberg ions.** (a) Two ions are confined by a harmonic trapping potential in the $X - Z$ plane. From the ground state $|g\rangle$, each ion is excited to the two Rydberg states $|\downarrow\rangle = |nS\rangle$ and $|\uparrow\rangle = |nP\rangle$. Due to different polarizabilities, ions in Rydberg states experience a state-dependent trapping potential along X, with frequencies $\omega_X^{\downarrow,\uparrow}$, and different equilibrium positions. When excited to the pair states $|\pi_1\rangle = |\uparrow\downarrow\rangle$ and $|\pi_2\rangle = |\downarrow\uparrow\rangle$, ions interact through the exchange interaction V_{ex}, whose strength depends on their separation r. A static offset electric field $\mathcal{E}$ allows to control the transverse equilibrium position of the ions. (b) The interplay between the exchange interaction and the state-dependent confinement shifts the energies of the states $|\pi_1\rangle$ (dashed curve) and $|\pi_2\rangle$ (solid curve). This results in a conical intersection in the potential energy surfaces U_- (red) and U_+ (blue) which, in the reference frame of the center of mass of the system, occurs at the ions' relative equilibrium separation $r_{x,z}^0$. See text for details.

each ion to a high-lying Rydberg level [32–41]. Moreover, due to the interplay between the state-dependent polarizability of Rydberg states and the radiofrequency electric field of the Paul trap, Rydberg ions feature a controllable state-dependent trapping potential [42, 43]. We show that this mechanism, in the presence of two different Rydberg states and combined with strong dipolar exchange interactions between two Rydberg ions, can be exploited to realize a minimal instance of a CI, consisting of two electronic states and two non-trivial

nuclear coordinates [2], shown in Fig. 1. The PESs and the position of the CI are controlled by the exchange interactions and an external electric field, allowing one to realize various scenarios which occur, e.g., in photo-chemical processes, but on nanometer length and microsecond time scales. The high degree of control over the vibrational motion of the ions makes it possible to minimize decoherence effects stemming from the coupling to additional rovibrational nuclear degrees of freedom. The latter, which cannot be avoided in real molecules, affects the dynamics across a CI on a sub-picoseconds timescale and hinders the experimental observation of coherent quantum effects [44–46]. To demonstrate the capabilities of our approach, we investigate effects induced by the GP in a feasible experimental setup: We show that the destructive interference between the paths encircling the different sides of a CI results in the localization of the nuclear wavepacket. This GP effect can be directly observed via a measurement of the electronic state population and does not require the spatially resolved detection of each ion.

Equations of motion.— We consider a system of two Rydberg ions of mass m in a linear Paul trap. The latter gives rise to an effective harmonic trapping potential with frequencies $\omega_{X,Y,Z}$ [42, 43, 47]. For the sake of simplicity, we assume $\omega_Y \gg \omega_X > \omega_Z$, so that the motion of the ions is confined to the $X-Z$ plane, with the Z−axis being the longitudinal one; see Fig. 1. The potential energy of the two trapped ions is $V_{\text{trap}} = m[\omega_X^2(X_1^2 + X_2^2) + \omega_Z^2(Z_1^2 + Z_2^2)]/2 + ke^2/r$, where the last term corresponds to the repulsive Coulomb interaction [with $k = 1/(4\pi\epsilon_0)$ being the Coulomb constant]. Here, $\boldsymbol{r} = \boldsymbol{R}_1 - \boldsymbol{R}_2$, with $\boldsymbol{R}_i = (X_i, Z_i)$, $i \in \{1, 2\}$, the nuclear coordinates in the laboratory frame. From their ground state $|g\rangle$, the ions can be excited to the two Rydberg levels $|nS\rangle = |\downarrow\rangle$ and $|nP\rangle = |\uparrow\rangle$, with n being the principal quantum number, both of which can be coupled by a microwave (MW) field with Rabi frequency Ω. Rydberg-excited ions interact via the exchange interaction potential $V_{\text{ex}}(r) \cdot (\sigma_+^1 \otimes \sigma_-^2 + \sigma_-^1 \otimes \sigma_+^2)$, with $\sigma_\pm^i$ acting on the i−th ion as $\sigma_+^i |\downarrow^i\rangle = |\uparrow^i\rangle$ and $\sigma_-^i |\uparrow^i\rangle = |\downarrow^i\rangle$. Furthermore, due to the large polarizability of Rydberg levels (denoted by ρ_σ, with $\sigma \in \{\downarrow, \uparrow\}$), ions in the Rydberg states experience an additional transverse trapping potential $\delta V_{\text{trap},\sigma} = -2\rho_\sigma A^2(X_1^2 + X_2^2)/m$, where A is the gradient of the radio-frequency field of the Paul trap [42, 43]. Finally, the transverse equilibrium positions of the ions is controlled via a static offset electric field $\mathcal{E}$ along the X−axis, which results in the potential energy contribution $V_{\text{mm}} = 2e\mathcal{E}(X_1 + X_2)$. In what follows we will focus on the dynamics in the spin subspace $\mathcal{H}_{\text{sp}}$, which is spanned by the ion pair states $|\pi_1\rangle = |\uparrow\downarrow\rangle$ and $|\pi_2\rangle = |\downarrow\uparrow\rangle$. The latter define the so-called *diabatic basis* of the system [30, 31]. In this subspace, we define the Pauli operators $S_0 = |\pi_1\rangle\langle\pi_1| + |\pi_2\rangle\langle\pi_2|$, $S_x = |\pi_1\rangle\langle\pi_2| + |\pi_2\rangle\langle\pi_1|$, and $S_z = |\pi_1\rangle\langle\pi_1| - |\pi_2\rangle\langle\pi_2|$.

The system is most conveniently analyzed in the center of mass (CM) reference frame, with $\boldsymbol{R} = (X, Z) = (\boldsymbol{R}_1 + \boldsymbol{R}_2)/2$ and $\boldsymbol{r} = (x, z)$ the CM and the relative coordinates, respec-

tively. In terms of the latter, the full system Hamiltonian is

$$H = \left(-\frac{\nabla_{\boldsymbol{R}}^2}{2M} - \frac{\nabla_{\boldsymbol{r}}^2}{2\mu}\right) \otimes S_0 + H_{\text{spin}}, \tag{1}$$

where the first term accounts for the total kinetic energy, with $M = 2m$ and $\mu = m/2$ the CM and reduced mass, respectively. The potential energy contributions are contained in $H_{\text{spin}} = H_{\text{spin}}^0 + H_{\text{spin}}^1$, with

$$H_{\text{spin}}^0 = (V_{\text{CM}} + V_{\text{rel}}) \otimes S_0, \tag{2a}$$

$$H_{\text{spin}}^1 = V_{\text{ex}}(r) \otimes S_x + H_{\text{CM−rel}}. \tag{2b}$$

Here, by defining the polarizabilities $\rho_\pm = \rho_\uparrow \pm \rho_\downarrow$, we have

$$V_{\text{CM}} = \frac{M}{2}\left(\omega_X^2 X^2 + \omega_Z^2 Z^2\right) + 2e\mathcal{E}X - A^2\rho_+ X^2, \tag{3a}$$

$$V_{\text{rel}} = \frac{\mu}{2}\left(\omega_X^2 x^2 + \omega_Z^2 z^2\right) + \frac{ke^2}{r} - A^2\rho_+ \frac{x^2}{4}. \tag{3b}$$

The terms in Eq. (3a) [Eq. (3b)] correspond to the trapping potential, the electrostatic potential associated with the static electric field $\mathcal{E}$ [the repulsive Coulomb potential], and the additional transverse trapping potential due to the Rydberg state-dependent polarizabilities, respectively. Finally, $H_{\text{CM−rel}} = A^2\rho_- Xx \otimes S_z$ describes the coupling between the electronic and nuclear motions arising from the unequal polarizabilities of the Rydberg states.

For typical experimental values of system parameters, H_{spin}^1 represents a small perturbation to H_{spin}^0. Hence, we first perform a harmonic approximation around the equilibrium positions of the ions as determined by H_{spin}^0, which are denoted by $\boldsymbol{R}^0 = (X^0, 0)$ and $\boldsymbol{r}^0 = (0, z_0)$. Then, by expanding H_{spin}^1 to the first order in the displacements $\boldsymbol{Q} = \boldsymbol{R} - \boldsymbol{R}^0$ and $\boldsymbol{q} = \boldsymbol{r} - \boldsymbol{r}^0$, we get

$$H_{\text{spin}} = S(\boldsymbol{Q}, \boldsymbol{q}) \otimes S_0 + G(\boldsymbol{Q}, \boldsymbol{q}) \otimes S_z + W(\boldsymbol{q}) \otimes S_x, \tag{4}$$

where $(\boldsymbol{Q}, \boldsymbol{q}) = (Q_x, Q_z, q_x, q_z)$ and

$$S(\boldsymbol{Q}, \boldsymbol{q}) = \frac{1}{2}M\boldsymbol{Q}^T \mathcal{K}^Q \boldsymbol{Q} + \frac{1}{2}\mu\boldsymbol{q}^T \mathcal{K}^q \boldsymbol{q}, \tag{5a}$$

$$G(\boldsymbol{Q}, \boldsymbol{q}) = \alpha^2\rho_-(Q_x + X^0)q_x, \tag{5b}$$

$$W(\boldsymbol{q}) = V_{\text{ex}}^0 + \nabla_{\boldsymbol{r}}V_{\text{ex}}(r)|_{\boldsymbol{r}=\boldsymbol{r}^0} \cdot \boldsymbol{q} \equiv V_{\text{ex}}^0 + F_z(\boldsymbol{r}^0)q_z. \tag{5c}$$

Here, we have introduced the dynamical matrices $\mathcal{K}_{\alpha\beta}^Q = M^{-1}\partial_{R_\alpha, R_\beta}V_{\text{CM}}|_{\boldsymbol{R}^0, \boldsymbol{r}^0}$ and $\mathcal{K}_{\alpha\beta}^q = \mu^{-1}\partial_{r_\alpha, r_\beta}V_{\text{rel}}|_{\boldsymbol{R}^0, \boldsymbol{r}^0}$, with $\alpha, \beta \in \{x, z\}$.

CIs occur at positions $(\boldsymbol{Q}^*, \boldsymbol{q}^*)$ such that $G(\boldsymbol{Q}^*, \boldsymbol{q}^*) = W(\boldsymbol{q}^*) = 0$ [2, 19]. From Eq. (5) we obtain two possibilities: $Q_x^* = -X^0, q_z^* = -V_{\text{ex}}^0/F_z(\boldsymbol{r}^0)$ or $q_x^* = 0, q_z^* = -V_{\text{ex}}^0/F_z(\boldsymbol{r}^0)$. The latter case is of particular interest since it can be studied entirely in the CM reference frame. This is seen as follows: a CI occurs in the *branching plane*, which is the subspace of the nuclear coordinates where the degeneracy between the PESs

is lifted linearly [48]. For a generic CI located at $(\boldsymbol{Q}^*, \boldsymbol{q}^*)$, the latter is spanned by the vectors $\boldsymbol{u} = \boldsymbol{g}(\boldsymbol{Q}^*, \boldsymbol{q}^*)/|\boldsymbol{g}(\boldsymbol{Q}^*, \boldsymbol{q}^*)|$ and $\boldsymbol{v} = \boldsymbol{w}(\boldsymbol{Q}^*, \boldsymbol{q}^*)/|\boldsymbol{w}(\boldsymbol{Q}^*, \boldsymbol{q}^*)|$, with

$$\boldsymbol{g}(\boldsymbol{Q}, \boldsymbol{q}) = \nabla_{\boldsymbol{Q}, \boldsymbol{q}} G(\boldsymbol{Q}, \boldsymbol{q}) = \alpha^2 \rho_-(q_x, 0, Q_x + X^0, 0), \quad (6a)$$

$$\boldsymbol{w}(\boldsymbol{Q}, \boldsymbol{q}) = \nabla_{\boldsymbol{Q}, \boldsymbol{q}} W(\boldsymbol{q}) = F_z(\boldsymbol{r}^0)(0, 0, 0, 1), \quad (6b)$$

being the gradients of $G(\boldsymbol{Q}, \boldsymbol{q})$ and $W(\boldsymbol{q})$. Considering the CI located at $\boldsymbol{q}^* = (0, -V_{\text{ex}}^0/F_z(\boldsymbol{r}^0))$, one finds $\boldsymbol{u} = (0, 0, 1, 0)$ and $\boldsymbol{v} = (0, 0, 0, 1)$. Hence, the corresponding branching plane coincides with the subspace of the relative nuclear coordinate and the position of the CI is not affected by the CM degrees of freedom. Two examples of PESs in the neighborhood of the CI are shown in Fig. 2 for different values of V_{ex}^0. Moreover, by denoting with $\ell_x^Q = (\hbar/M\mathcal{K}_{xx}^Q)^{1/2}$ the characteristic oscillation length associated with the motion of the CM, one typically finds $X_0 \gg \ell_x^Q$. Thus, along the transverse direction, the CM performs small oscillations around its equilibrium position X^0 which, in turn, results only in a little deformation of the PESs. To inspect the main effects induced by the CI we can therefore neglect the motion of the CM, set $\boldsymbol{Q} = 0$ in Eq. (5), and hereinafter omit the dependence from $\boldsymbol{Q}$.

CI induced dynamics in the nuclear motion.— In the spirit of the Born-Huang approach [49], the nuclear motion of the ions is determined by the PESs given by the eigenvalues of the electronic Hamiltonian of Eq. (4),

$$U_\pm(\boldsymbol{q}) = S(\boldsymbol{q}) \pm \sqrt{[G(\boldsymbol{q})]^2 + [W(\boldsymbol{q})]^2}, \quad (7)$$

where the coordinates of the ions are treated as fixed parameters. The corresponding eigenstates, which define the electronic *adiabatic basis*, are given by [30, 31]

$$|\varphi_+(\boldsymbol{q})\rangle = \cos[\Lambda(\boldsymbol{q})] |\pi_1\rangle + \sin[\Lambda(\boldsymbol{q})] |\pi_2\rangle, \quad (8a)$$

$$|\varphi_-(\boldsymbol{q})\rangle = -\sin[\Lambda(\boldsymbol{q})] |\pi_1\rangle + \cos[\Lambda(\boldsymbol{q})] |\pi_2\rangle, \quad (8b)$$

where $\Lambda(\boldsymbol{q})$ is fixed by $\tan[2\Lambda(\boldsymbol{q})] = W(\boldsymbol{q})/G(\boldsymbol{q})$. Note that if $\boldsymbol{q}$ is varied along a close path encircling the CI, the angle $\Lambda(\boldsymbol{q})$ changes only by π instead of 2π: the states $|\varphi_\pm(\boldsymbol{q})\rangle$ acquire an extra phase of π, known as the GP [14, 15, 19].

For the sake of simplicity, we first consider a suitably tailored exchange interaction potential such that $V_{\text{ex}}^0 = 0$ [40, 50]. In this case, the CI occurs at $\boldsymbol{q}^* = 0$ and the PESs, shown in Fig. 2(a), are symmetric under the reflections $\boldsymbol{q} \to -\boldsymbol{q}$. As a consequence, the two paths connecting the two minima of $U_-(\boldsymbol{q})$ and encircling the CI from opposite sides are identical. This represents the ideal setting to investigate dynamical effects induced by the presence of a CI and, in particular, those related to the GP. To do so, we consider the following protocol: First, we excite adiabatically both ions from the ground state $|g\rangle$ to the $|\downarrow\rangle$ Rydberg state (see Fig. 1). In the CM reference frame, the corresponding equilibrium nuclear wavefunction $\phi_{\text{rel}}^{\text{ss}}(\boldsymbol{q})$ is a Gaussian centered around $(q_{x,\text{ss}}^0, 0)$ [50]. Here, we set $q_{x,\text{ss}}^0$ so that $\phi_{\text{rel}}^{\text{ss}}(\boldsymbol{q})$ is peaked in one of the two minima of $U_-(\boldsymbol{q})$ [see Fig. 2(a)]. As explained in the Supplemental Material (SM) [50], this allows us to maximize the visibility of the
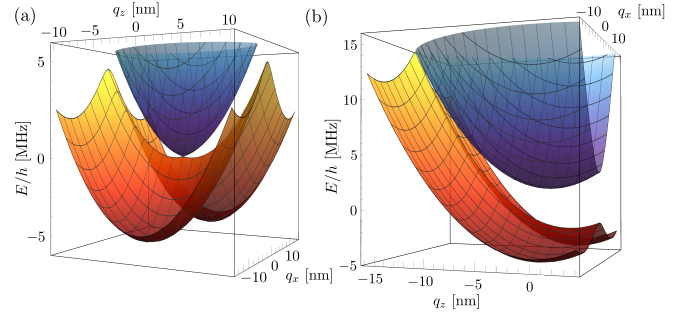

FIG. 2. **Potential energy surfaces in the branching plane.** Plot of the eigenvalues of Eq. (4) (i.e., the PESs) $U_\pm(\boldsymbol{q})$ as a function of the displacements q_x and q_z. (a) For $V_{\text{ex}}^0/h = 0$, a CI occurs at $\boldsymbol{q}^* = (0, 0)$ while for (b) $V_{\text{ex}}^0/h = 2\pi \times 0.3$ MHz the CI is shifted to $\boldsymbol{q}^* = (0, -V_{\text{ex}}^0/F_z(\boldsymbol{r}^0))$ (see text for details). Here, we considered ^{88}Sr$^+$ Rydberg ions, with $m = 87.9 \times 1.66 \times 10^{-27}$ Kg, and set $\omega_X = 2\pi \times 1.6$ MHz, $\omega_Z = 2\pi$ MHz, $\mathcal{E} = 2.529$ V/m (resulting in $X^0 = -0.024$ μm), $\rho_\downarrow = 8.9 \times 10^{-31}$ C^{2}m^2/J, $\rho_\uparrow = -3.8 \times 10^{-30}$ C^{2}m^2/J (corresponding to Rydberg $|nS\rangle$ and $|nP\rangle$ states with $n = 50$), and $F_z(\boldsymbol{r}^0) = 2\pi \times 20$ MHz/μm.

GP effects thanks to symmetries of the system. Then, to initiate the dynamics in the spin subspace $\mathcal{H}_{\text{sp}}$, we temporarily turn on a MW field coupling the $|\downarrow\rangle$ and $|\uparrow\rangle$ states (see Fig. 1) in such a way that the electronic state is fully transferred to the lower PES eigenstate $|\varphi_-(\boldsymbol{q})\rangle$. After that, the MW field is turned off. The subsequent dynamics in the subspace $\mathcal{H}_{\text{sp}}$ is then governed by $H_{\text{rel}} = -\nabla_{\boldsymbol{q}}^2/(2\mu) \otimes S_0 + H_{\text{spin}}$ [see Eqs. (4) and (5)], with the initial state given by $|\psi_0(\boldsymbol{q})\rangle = |\psi(\boldsymbol{q}, t = 0)\rangle = \phi_{\text{rel}}^{\text{ss}}(\boldsymbol{q}) |\varphi_-(\boldsymbol{q})\rangle$.

We now inspect the time evolution of the populations of the two PESs, $\tilde{n}_\mu(t)$, and of the diabatic basis states, $n_k(t)$. These can be obtained by expanding the full time dependent wavefunction as

$$|\psi(\boldsymbol{q}, t)\rangle = \sum_{k=1,2} \phi_k(\boldsymbol{q}, t) |\pi_k\rangle = \sum_{\mu=\pm} \tilde{\phi}_\mu(\boldsymbol{q}, t) |\varphi_\mu(\boldsymbol{q})\rangle, \quad (9)$$

where the coefficients $\phi_k(\boldsymbol{q}, t)$ [$\tilde{\phi}_\mu(\boldsymbol{q}, t)$] represent the diabatic (adiabatic) nuclear wavefunction components. Hence, the populations of the diabatic and adiabatic states are given by $n_k(t) = \int |\phi_k(\boldsymbol{q}, t)|^2 \, d^2\boldsymbol{q}$ and $\tilde{n}_\mu(t) = \int |\tilde{\phi}_\mu(\boldsymbol{q}, t)|^2 \, d^2\boldsymbol{q}$, respectively.

To identify the effects induced by the CI, we compare the exact dynamics of the system, which takes into account the presence of the two crossing PESs, with a BO approximation, in which the nuclear motion takes place on the lower PES only. In both cases, the nuclear dynamics is obtained by solving numerically the time-dependent Schrödinger equation associated with H_{rel} in the diabatic representation via a Crank-Nicholson scheme [50, 51].

In the BO approximation, the nuclei oscillate around the equilibrium position $\boldsymbol{r}^0$ of the relative motion and in the CM reference frame the nuclear density $\mathcal{N}(\boldsymbol{q}, t) = \sum_k |\phi_k(\boldsymbol{q}, t)|^2$ moves from one minimum of $U_-(\boldsymbol{q})$ to the other. The effects of this motion can be directly observed in the time evolution of the diabatic populations $n_k(t)$, which can be monitored
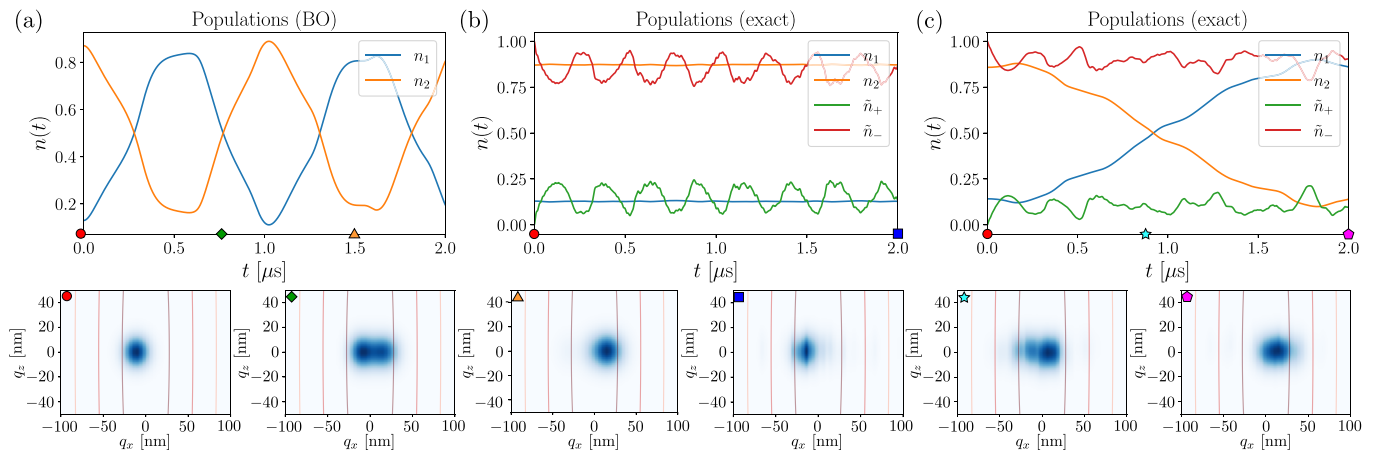
FIG. 3. **Dynamics of the diabatic and adiabatic populations.** Time evolution of the populations $n_k(t)$ of the diabatic states $|\pi_1\rangle$ (blue curve) and $|\pi_2\rangle$ (yellow curve) in the (a) BO approximation, (b) exact dynamics with $V_{ex}^0/h = 0$, and (c) exact dynamics with $V_{ex}^0/h = 2\pi \times 0.3$ MHz. In (b, c), the populations of the adiabatic states, $\tilde{n}_-(t)$ (red curves) and $\tilde{n}_+(t)$ (green curves) are also shown. (b): The complete destructive interference between the two paths surrounding the CI results in the freezing of the nuclear motion in the CM reference frame. (c): A finite V_{ex}^0 shifts the CI and breaks the perfect symmetry between the two paths observed in (b). As a consequence, the nuclear wavepacket can move to the other local minimum of $U_-(\boldsymbol{q})$ and the diabatic populations $n_k(t)$ swap with each other. The bottom row illustrates some snapshots of the dynamics of the nuclear density $\mathcal{N}(\boldsymbol{q}, t)$ in the CM reference frame associated with the various time evolutions shown in the upper row (see the corresponding marks). Here, red contours display the behavior of $|U_+(\boldsymbol{q}) - U_-(\boldsymbol{q})|$, with darker tones corresponding to $|U_+(\boldsymbol{q}) - U_-(\boldsymbol{q})| \to 0$. In all panels, the system is initialized in the state $|\psi_0(\boldsymbol{q})\rangle$, with $q_{x,ss}^0 = -0.011$ μm. Other parameters are as in Fig. 2.

in real-time via a spectroscopic measurement of the Rydberg states. As shown in Fig. 3(a), the oscillatory motion of the nuclear density gives rise to large oscillations in $n_k(t)$. This changes drastically when the exact dynamics in the presence of the CI at $\boldsymbol{q}^* = \boldsymbol{0}$ is considered. Due to the symmetry of the PESs, in moving from one minimum of $U_-(\boldsymbol{q})$ to the other, the nuclear wavepacket splits evenly on the two paths encircling the CI on the opposite sides. The relative GP accumulated in this motion around the CI on the two paths differs by π and results in a perfect destructive interference at the other minimum of $U_-(\boldsymbol{q})$. As a consequence, the nuclei are inhibited from moving: the nuclear density $\mathcal{N}(\boldsymbol{q}, t)$ is stuck in the initial minimum of $U_-(\boldsymbol{q})$. This has direct impact on the diabatic populations, shown in Fig. 3(b), which exhibit only small oscillations around their initial values.

To confirm that the observed behavior is entirely due to the GP, we have also considered a BO approximation in which the diagonal BO correction terms have also been included. The latter take into account the additional potential energy barrier induced by the presence of the CI [19, 52]. As shown in the SM [50], the inclusion of the diagonal BO correction does not prevent the oscillatory dynamics of the nuclei (and of diabatic populations) but only results in a slight increase of the period of the oscillations.

Controlling the CI.— So far we considered the case in which the CI is located at the saddle point of $U_-(\boldsymbol{q})$ and the PESs are highly symmetric around the CI. This was achieved with a fine-tuned exchange interaction potential, such that $V_{ex}^0 = 0$. We now examine the more general case with $V_{ex}^0 \neq 0$. This leads to a scenario common to many real molecules, in which CIs are located on the slope of (asymmetric) PESs [53–55].

As shown in Eq. (5c), a finite value of V_{ex}^0 allows one to control the coordinate q_z^* of the CI. In this case, the symmetry of the PESs around the CI is broken and the paths encircling the two sides of the CI are no longer equivalent [Fig. 2(b)]. This provides a clear demonstration of the fact that the freezing of the nuclear motion is due to a perfect destructive interference caused by a GP. Indeed, when $V_{ex}^0 \neq 0$, the initial nuclear wavefunction splits in two wavepackets with different weights and the interference between the two paths encircling the CI occurs only partially. As a consequence, the nuclear density $\mathcal{N}(\boldsymbol{q}, t)$ can now move from one minimum of $U_-(\boldsymbol{q})$ to the other and the time evolution of the diabatic populations differs significantly from the one of Fig. 3(b): as shown in Fig. 3(c), $n_1(t)$ and $n_2(t)$ oscillate and swap with each other after a time interval proportional to V_{ex}^0.

Conclusions.— We have demonstrated that a minimal setup of two trapped Rydberg ions can be exploited to engineer a CI in a highly tunable system. An external static electric field and a tailored exchange interaction potential between Rydberg states fully control the shape of the two crossing PESs and the location of the CI. The high degree of control on the electronic and vibrational states of the ions makes it possible to simulate the dynamics of a wavepacket around the CI. We have shown that interference effects due to the GP near a CI inhibit the movement of nuclear wavepackets. This phenomenon has a direct impact on the populations of the Rydberg states and can thus be readily observed through a spectroscopic measurement. Extending this study to many-ion systems would make it possible to analyze the dynamics near CIs in more complex environments, such as in the presence of dissipation induced by coupling to many phonon modes [44–

46].

---

[1] M. Born and R. Oppenheimer, Ann. Phys. **389**, 457 (1927).

[2] W. Domcke, D. R. Yarkony, and H. Köppel, *Conical Intersections. Electronic structure, Dynamics and Spectroscopy.* (Word Scientific, Singapore, 2004).

[3] J. C. Tully, J. Chem. Phys. **137**, 22A301 (2012).

[4] D. R. Yarkony, Rev. Mod. Phys. **68**, 985 (1996).

[5] M. Baer, *Beyond Born-Oppenheimer. Conical Intersections and Electronic Nonadiabatic Coupling Terms* (Wiley-Interscience, Hoboken, 2006).

[6] N. Ismail, L. Blancafort, M. Olivucci, B. Kohler, and M. A. Robb, J. Am. Chem. Soc **124**, 6818 (2002).

[7] S. Perun, A. L. Sobolewski, and W. Domcke, J. Am. Chem. Soc **127**, 6257 (2005).

[8] M. Barbatti, A. J. A. Aquino, J. J. Szymczak, D. Nachtigallová, P. Hobza, and H. Lischka, Proc. Natl. Acad. Sci. U.S.A. **107**, 21453 (2010).

[9] R. Schoenlein, L. Peteanu, R. Mathies, and C. Shank, Science **254**, 412 (1991).

[10] D. Polli, P. Altoè, O. Weingart, K. M. Spillane, C. Manzoni, D. Brida, G. Tomasello, G. Orlandi, P. Kukura, R. A. Mathies, M. Garavelli, and G. Cerullo, Nature **467**, 440 (2010).

[11] S. Rinaldi, F. Melaccio, S. Gozem, F. Fanelli, and M. Olivucci, Proc. Natl. Acad. Sci. U.S.A. **111**, 1714 (2014).

[12] L. Hammarström and S. Styring, Philos. Trans. R. Soc. B **363**, 1283 (2008).

[13] A. Bohm, A. Mostafazadeh, H. Koizumi, Q. Niu, and J. Zwanziger, *The Geometric Phase in Quantum Systems* (Springer-Verlag, Berlin, 2003).

[14] H. C. Longuet-Higgins, U. Öpik, M. H. L. Pryce, and R. A. Sack, Proc. R. Soc. Lond. A **244**, 1 (1958).

[15] M. V. Berry, Proc. R. Soc. Lond. A **392**, 45 (1984).

[16] C. A. Mead, Rev. Mod. Phys. **64**, 51 (1992).

[17] S. C. Althorpe, T. Stecher, and F. Bouakline, J. Chem. Phys. **129**, 214117 (2008).

[18] I. G. Ryabinkin and A. F. Izmaylov, Phys. Rev. Lett. **111**, 220406 (2013).

[19] I. G. Ryabinkin, L. Joubert-Doriol, and A. F. Izmaylov, Acc. Chem. Res. **50**, 1785 (2017).

[20] H.-D. Meyer, F. Gatti, and G. A. Worth, *Multidimensional Quantum Dynamics.* (Wiley-VCH, Weinheim, 2009).

[21] A. D. G. Nunn, R. S. Minns, R. Spesyvtsev, M. J. Bearpark, M. A. Robb, and H. H. Fielding, Phys. Chem. Chem. Phys. **12**, 15751 (2010).

[22] M. Kowalewski, K. Bennett, K. E. Dorfman, and S. Mukamel, Phys. Rev. Lett. **115**, 193003 (2015).

[23] S. Adachi, T. Schatteburg, A. Humeniuk, R. Mitrić, and T. Suzuki, Phys. Chem. Chem. Phys. **21**, 13902 (2019).

[24] L. Young, K. Ueda, M. Gühr, P. H. Bucksbaum, M. Simon, S. Mukamel, N. Rohringer, K. C. Prince, C. Masciovecchio, M. Meyer, A. Rudenko, D. Rolles, C. Bostedt, M. Fuchs, D. A. Reis, R. Santra, H. Kapteyn, M. Murnane, H. Ibrahim, F. Légaré, M. Vrakking, M. Isinger, D. Kroon, M. Gisselbrecht, A. L'Huillier, H. J. Wörner, and S. R. Leone, J. of Phys. B: At. Mol. and Opt. Phys. **51**, 032003 (2018).

[25] M. Šindelka, N. Moiseyev, and L. S. Cederbaum, J. of Phys. B: At. Mol. and Opt. Phys. **44**, 045603 (2011).

[26] N. Moiseyev, M. Šindelka, and L. S. Cederbaum, J. of Phys. B: At. Mol. and Opt. Phys. **41**, 221001 (2008).

[27] A. O. G. Wallis, S. A. Gardiner, and J. M. Hutson, Phys. Rev. Lett. **103**, 083201 (2009).

[28] T. F. Gallagher, *Rydberg atoms* (Cambridge University Press, New York, 2005).

[29] R. Löw, H. Weimer, J. Nipper, J. B. Balewski, B. Butscher, H. P. Büchler, and T. Pfau, J. of Phys. B: At. Mol. and Opt. Phys. **45**, 113001 (2012).

[30] S. Wüster, A. Eisfeld, and J. M. Rost, Phys. Rev. Lett. **106**, 153002 (2011).

[31] S. Wüster and J.-M. Rost, J. of Phys. B: At. Mol. and Opt. Phys.Phys. **51**, 032001 (2018).

[32] M. Müller, L. Liang, I. Lesanovsky, and P. Zoller, New J. Phys. **10**, 093009 (2008).

[33] F. Schmidt-Kaler, T. Feldker, D. Kolbe, J. Walz, M. Müller, P. Zoller, W. Li, and I. Lesanovsky, New J. Phys. **13**, 075014 (2011).

[34] W. Li and I. Lesanovsky, Phys. Rev. Lett. **108**, 023003 (2012).

[35] W. Li and I. Lesanovsky, Appl. Phys. B **114**, 37 (2014).

[36] G. Higgins, W. Li, F. Pokorny, C. Zhang, F. Kress, C. Maier, J. Haag, Q. Bodart, I. Lesanovsky, and M. Hennrich, Phys. Rev. X **7**, 021038 (2017).

[37] G. Higgins, F. Pokorny, C. Zhang, Q. Bodart, and M. Hennrich, Phys. Rev. Lett. **119**, 220501 (2017).

[38] A. Mokhberi, J. Vogel, J. Andrijauskas, P. Bachor, J. Walz, and F. Schmidt-Kaler, J. of Phys. B: At. Mol. and Opt. Phys. **52**, 214001 (2019).

[39] J. Vogel, W. Li, A. Mokhberi, I. Lesanovsky, and F. Schmidt-Kaler, Phys. Rev. Lett. **123**, 153603 (2019).

[40] F. M. Gambetta, C. Zhang, M. Hennrich, I. Lesanovsky, and W. Li, Phys. Rev. Lett. **125**, 133602 (2020).

[41] C. Zhang, F. Pokorny, W. Li, G. Higgins, A. Pöschl, I. Lesanovsky, and M. Hennrich, Nature **580**, 345 (2020).

[42] G. Higgins, F. Pokorny, C. Zhang, and M. Hennrich, Phys. Rev. Lett. **123**, 153602 (2019).

[43] G. Higgins, *A Single Trapped Rydberg Ion* (Springer, Cham, 2019).

[44] A. Kühl and W. Domcke, J. Chem. Phys. **116**, 263 (2001).

[45] L. Chen, M. F. Gelin, V. Y. Chernyak, W. Domcke, and Y. Zhao, Faraday Discuss. **194**, 61 (2016).

[46] R. Ulbricht, S. Dong, I.-Y. Chang, B. M. K. Mariserla, K. M. Dani, K. Hyeon-Deuk, and Z.-H. Loh, Nat. Commun. **7**, 13510 (2016).

[47] F. G. Major, V. N. Gheorghe, and G. Werth, *Charged Particle Traps*, Vol. 1 (Springer-Verlag, Berlin, 2005).

[48] D. R. Yarkony, in *Conical Intersections. Electronic structure, Dynamics and Spectroscopy.*, edited by W. Domcke, D. R. Yarkony, and H. Köppel (Word Scientific, Singapore, 2004).

[49] M. Born and K. Huang, *Dynamical Theory of Crystal Lattices* (Clarendon Press, Oxford, 1954).

[50] See Supplemental Material for details on the preparation of the nuclear initial state $\phi_{\text{rel}}^{\text{ss}}(q)$, the tailored exchange interaction potential $V_{\text{ex}}(r)$, and the BO approximations.

[51] J. W. Thomas, *Numerical Partial Differential Equations: Finite Difference Methods*, Vol. 1 (Springer-Verlag, New York, 1995).

[52] R. Gherib, L. Ye, I. G. Ryabinkin, and A. F. Izmaylov, J. Chem. Phys. **144**, 154103 (2016).

[53] B. G. Levine and T. J. Martínez, Annu. Rev. Phys. Chem. **58**, 613 (2007).

[54] J. Yang, X. Zhu, T. J. A. Wolf, Z. Li, J. P. F. Nunes, R. Coffee, J. P. Cryan, M. Gühr, K. Hegazy, T. F. Heinz, K. Jobe, R. Li, X. Shen, T. Veccione, S. Weathersby, K. J. Wilkin, C. Yoneda, Q. Zheng, T. J. Martinez, M. Centurion, and X. Wang, Science **361**, 64 (2018).

[55] K. F. Chang, M. Reduzzi, H. Wang, S. M. Poullain, Y. Kobayashi, L. Barreau, D. Prendergast, D. M. Neumark, and S. R. Leone, Nat. Commun. **11**, 4042 (2020).

Supplemental Material for "Exploring the many-body dynamics near a conical intersection with trapped Rydberg ions"

In this Supplemental Material we provide additional details on the preparation of the initial state for the system dynamics of Fig. 3 of the main text, the tailored exchange interaction potential used in Eq. (5) of the main text, and the inclusion of the diagonal contributions to the Born-Oppenheimer approximation.

INITIALIZATION OF THE NUCLEAR WAVEPACKET

In this section, we discuss the initialization protocol for the two-ion system for the dynamics shown in Fig. 3 of the main text. First, both the ions are excited from their ground state $|g\rangle$ to the $|\downarrow\rangle = |nS\rangle$ state. Here, the full system Hamiltonian has the same form as Eq. (1) of the main text,

$$H^{\text{ss}} = \left(-\frac{\nabla_R^2}{2M} - \frac{\nabla_r^2}{2\mu}\right) \otimes S_0 + H_{\text{spin}}^{\text{ss}}, \tag{S1}$$

but without the exchange interaction and the coupling between the centre of mass (CM) and relative coordinates. In particular,

$$H_{\text{spin}}^{\text{ss}} = (V_{\text{CM}} + V_{\text{rel}}) \otimes S_0, \tag{S2}$$

with

$$V_{\text{CM}}^{\text{ss}} = \frac{M}{2}\left(\omega_X^2 X^2 + \omega_Z^2 Z^2\right) + 2e\mathcal{E}X - 2\alpha^2\rho_s X^2, \tag{S3a}$$

$$V_{\text{rel}}^{\text{ss}} = \frac{\mu}{2}\left(\omega_X^2 x^2 + \omega_Z^2 z^2\right) + \frac{ke^2}{r} - 2A^2\rho_s\frac{x^2}{4}. \tag{S3b}$$

The CM and relative equilibrium positions of the ions, R_{ss}^0 and r_{ss}^0, respectively, are determined by the solutions of the equations $\nabla_R V_{\text{CM}}^{\text{ss}}|_{R_{\text{ss}}^0} = 0$ and $\nabla_r V_{\text{rel}}^{\text{ss}}|_{r_{\text{ss}}^0} = 0$. By symmetry consideration, they can be written as $R_{\text{ss}}^0 = (X_{\text{ss}}^0, 0)$ and $r_{\text{ss}}^0 = (0, z_{\text{ss}}^0)$. Here, X_{ss}^0 depends on the external electric field $\mathcal{E}$ while z_{ss}^0 is determined by the interplay between the Coulomb repulsion and the trapping potential. Expanding Eq. (S3) around ions' equilibrium positions and defining the CM and relative displacements from the latter as $Q_{\text{ss}} = R_{\text{ss}} - R_{\text{ss}}^0$ and $q_{\text{ss}} = r - r_{\text{ss}}^0$, one gets

$$V_{\text{CoM}}^{\text{ss}} + V_{\text{rel}}^{\text{ss}} \approx \frac{1}{2}MQ_{\text{ss}}^T \mathcal{K}_{\text{ss}}^Q Q_{\text{ss}} + \frac{1}{2}\mu q_{\text{ss}}^T \mathcal{K}_{\text{ss}}^q q_{\text{ss}}, \tag{S4}$$

where the dynamical matrices $\mathcal{K}_{\text{ss}}^Q$ and $\mathcal{K}_{\text{ss}}^q$ are given by

$$(\mathcal{K}_{\text{ss}}^Q)_{\alpha\beta} = \frac{1}{M}\frac{\partial^2 V_{\text{CoM}}^{\text{ss}}}{\partial R_\alpha \partial R_\beta}\bigg|_{R_{\text{ss}}^0, r_{\text{ss}}^0} \quad \text{and} \quad (\mathcal{K}_{\text{ss}}^q)_{\alpha\beta} = \frac{1}{\mu}\frac{\partial^2 V_{\text{rel}}^{\text{ss}}}{\partial r_\alpha \partial r_\beta}\bigg|_{R_{\text{ss}}^0, r_{\text{ss}}^0}. \tag{S5}$$

In particular, from Eq. (S3) we obtain

$$\mathcal{K}_{\text{ss}}^Q = \begin{pmatrix} \omega_X^2 - \frac{4A^2}{M}\rho_s & 0 \\ 0 & \omega_Z^2 \end{pmatrix}, \tag{S6a}$$

$$\mathcal{K}_{\text{ss}}^q = \begin{pmatrix} \omega_X^2 - \frac{\alpha^2}{\mu}\rho_s - \frac{ke^2}{\mu|z_{\text{ss}}^0|^3} & 0 \\ 0 & \omega_Z^2 + \frac{2ke^2}{\mu|z_{\text{ss}}^0|^3} \end{pmatrix}. \tag{S6b}$$

Therefore, being $\mathcal{K}_{ss}^Q$ and $\mathcal{K}_{ss}^q$ diagonal, Eq. (S4) can be written as a sum of harmonic potentials with renormalized trapping frequencies,

$$V_{\text{CoM}} + V_{\text{rel}} \approx \frac{1}{2} M \left[\left(\tilde{\omega}_X^Q \right)^2 Q_{ss,x}^2 + \left(\tilde{\omega}_Z^Q \right)^2 Q_{ss,z}^2 \right] + \frac{1}{2} \mu \left[\left(\tilde{\omega}_X^q \right)^2 q_{ss,x}^2 + \left(\tilde{\omega}_Z^q \right)^2 q_{ss,z}^2 \right], \tag{S7}$$

where

$$\tilde{\omega}_X^Q = \sqrt{\omega_X^2 - \frac{4A^2}{M} \rho_s}, \quad \tilde{\omega}_Z^Q = \omega_Z, \quad \tilde{\omega}_X^q = \sqrt{\omega_X^2 - \frac{\alpha^2}{\mu} \rho_s - \frac{ke^2}{\mu |z_{ss}^0|^3}}, \quad \text{and} \quad \tilde{\omega}_Z^q = \sqrt{\omega_Z^2 + \frac{2ke^2}{\mu |z_{ss}^0|^3}}. \tag{S8}$$

The (nuclear) ground-state wavefunction associated with this potential is thus given by

$$\Phi^{\text{ss}}(Q, q) = \phi_{\text{CoM}}^{\text{ss}}(Q) \phi_{\text{rel}}^{\text{ss}}(q), \tag{S9}$$

with

$$\phi_{\text{CoM}}^{\text{ss}}(Q) = \frac{\exp\left[-\frac{1}{2} \left(\frac{Q_x}{\ell_{ss,x}^Q} \right)^2 - \frac{1}{2} \left(\frac{Q_z}{\ell_{ss,z}^Q} \right)^2 \right]}{\sqrt{\pi \ell_{ss,x}^Q \ell_{ss,z}^Q}} \quad \text{and} \quad \phi_{\text{rel}}^{\text{ss}}(q) = \frac{\exp\left[-\frac{1}{2} \left(\frac{q_x - q_x^0}{\ell_{ss,x}^q} \right)^2 - \frac{1}{2} \left(\frac{q_z}{\ell_{ss,z}^q} \right)^2 \right]}{\sqrt{\pi \ell_{ss,x}^q \ell_{ss,z}^q}}, \tag{S10}$$

where $\ell_{ss,\alpha}^Q = (\hbar/M\tilde{\omega}_\alpha^Q)^{1/2}$ and $\ell_{ss,\alpha}^q = (\hbar/\mu\tilde{\omega}_\alpha^q)^{1/2}$ are the typical harmonic oscillator lengthscales. In Eq. (S10), we have also included the displacements $q_{ss,x}^0$, which is crucial for the investigation of the effects induced by the conical intersection (CI) in the main text. The latter can be achieved, e.g., by exciting the transverse breathing mode of the two-ion system or by modifying the electric field $\mathcal{E} = (\mathcal{E}, 0)$ to $\mathcal{E} = (\mathcal{E} + Cx, Cz)$, with C being a constant. In the latter case, it is possible to show that in order to obtain a finite $q_{ss,x}^0$ of the order of few nanometers the corrections to the analysis above [and, in particular, to Eq. (S6)] are negligible.

We conclude this section by discussing the relationship between the initial Gaussian nuclear wavefunction and the symmetry properties of the system. We recall that, in the CM reference frame and neglecting the motion of the CM, the dynamics of the system is governed by $H_{\text{rel}} = -\nabla_q^2/(2\mu) \otimes S_0 + H_{\text{spin}}$, with H_{spin} given in Eq. (1) of the main text. In general, the eigenstates of H_{rel} are given by

$$H_{\text{rel}} \left| \psi^E(q) \right\rangle = E \left| \psi^E(q) \right\rangle, \tag{S11}$$

with $\left| \psi^E(q) \right\rangle$ belonging to the Hilbert space $\mathcal{H} = \mathcal{H}_q \otimes \mathcal{H}_{\text{spin}}$. In the adiabatic representation, the eigenstate $\left| \psi^E(q) \right\rangle$ can be written as

$$\left| \psi^E(q) \right\rangle = \sum_{\mu=\pm} \tilde{\phi}_\mu^E(q) \left| \varphi_\mu(q) \right\rangle, \tag{S12}$$

with $\left| \varphi_\mu(q) \right\rangle$ defined in Eq. (8) of the main text. The functions $\tilde{\phi}_\mu^E(q)$ are called nuclear wavefunctions, despite one has to keep in mind that they are not proper wavefuctions on $\mathcal{H}_q$ [13].

From Eq. (5) of the main one can verify that, for $V_{\text{ex}}^0 = 0$, the parity operator $\mathcal{P}$ implementing the spatial reflection $q \to -q$ is a symmetry of the system, i.e., $[H_{\text{ref}}, \mathcal{P}] = 0$. Therefore, it is possible to find a basis in $\mathcal{H}$, denoted by $\{ \left| \chi_+^E(q) \right\rangle, \left| \chi_-^E(q) \right\rangle \}$, such that

$$H_{\text{rel}} \left| \chi_\pm^E(q) \right\rangle = E \left| \chi_\pm^E(q) \right\rangle, \tag{S13a}$$

$$\mathcal{P} \left| \chi_\pm^E(q) \right\rangle = \pm \left| \chi_\pm^E(q) \right\rangle, \tag{S13b}$$

where, in the adiabatic basis,

$$\left| \chi_\pm^E(q) \right\rangle = \sum_{\mu=\pm} \tilde{\xi}_{\mp,\mu}^E(q) \left| \varphi_\mu(q) \right\rangle. \tag{S14}$$

Due to the presence of the CI at $q = 0$ and of the associated geometric phase, one has $\mathcal{P} \left| \varphi_\mu(q) \right\rangle = - \left| \varphi_\mu(q) \right\rangle$, $\forall q$. Therefore, to preserve the single-valuedness of $\left| \chi_\pm^E(q) \right\rangle$, the functions $\tilde{\xi}_{\pm,\mu}^E(q)$ must obey the identity $\mathcal{P} \tilde{\xi}_{\pm,\mu}^E(q) = \mp \tilde{\xi}_{\pm,\mu}^E(q)$, i.e., $\tilde{\xi}_{+,\mu}^E(q)$ [$\tilde{\xi}_{-,\mu}^E(q)$] is even (odd) with respect to the transformation $q \to -q$.

We can now focus on the initial state, $|\psi_0(q)\rangle = \phi_{\text{rel}}^{\text{ss}}(q)\,|\varphi_-(q)\rangle$. Since $\phi_{\text{rel}}^{\text{ss}}(q)$ is a Gaussian peaked in one of the two minima of the lower potential energy surface (PES), the initial state $|\psi_0(q)\rangle$ can be expanded to a high degree of approximation on the basis $\{|\chi_+^E(q)\rangle, |\chi_-^E(q)\rangle\}$ as

$$|\psi_0(q)\rangle \approx \sum_E c_E(0)\left(|\chi_+^E(q)\rangle + |\chi_-^E(q)\rangle\right), \tag{S15}$$

with $c_E(0)$ a given coefficient. Note that the choice of the sign between the $|\chi_\pm^E(q)\rangle$ states is arbitrary and the expansion with the $-$ sign would result in the state in which the nuclear wavefunction is centered in the other minimum of $U_-(q)$. Indeed, the equally weighted superpositions $\tilde{\xi}_{+,\mu}^E(q) \pm \tilde{\xi}_{-,\mu}^E(q)$ are non-vanishing in one of the two minima of $U_-(q)$ only. Since $|\chi_\pm(q)\rangle$ are eigenstates of H_{rel}, the initial wavefunction $|\psi_0(q)\rangle$ evolves in time as

$$|\psi_0(q,t)\rangle \approx \sum_E c_E(t)\left(|\chi_+^E(q)\rangle + |\chi_-^E(q)\rangle\right), \tag{S16}$$

with $c_E(t) = e^{iEt}c_E(0)$. This implies that $|\psi_0(q,t)\rangle$ is an equally weighted superposition of $|\chi_+^E(q)\rangle$ and $|\chi_-^E(q)\rangle$ $\forall t$ and, hence, it remains in the same minimum of $U_-(q)$ up to very long timescales.

In the case with $V_{\text{ex}}^0 \neq 0$, $\mathcal{P}$ is no longer a symmetry of the system and, in general, its eigenstates $|\chi_\pm(q)\rangle$ are not eigenstates of H_{rel}. Thus, the time evolved initial nuclear wavepacket cannot be written in the form of Eq. (S16): $|\psi_0(q,t)\rangle$ is not an equally weighted superposition of the states $|\chi_\pm(q)\rangle$ and, in general, it is not constrained to remain in one of the minima of $U_-(q)$.

MICROWAVE DRESSED EXCHANGE POTENTIAL

In this section we provide additional details about the microwave (MW) dressing scheme employed to engineer the exchange interaction potential $V_{\text{ex}}(r)$ we used in Eq. (5) of the main text. We consider a pair of $^{88}\text{Sr}^+$ trapped Rydberg ions, and focus on their Rydberg states $|nS\rangle = |\downarrow\rangle = (0, 1)^T$ and $|nP\rangle = |\uparrow\rangle = (1, 0)^T$ (with n a positive integer). The latter interact through a conventional exchange interaction potential

$$\mathcal{V}_{\text{ex}} = \tilde{V}_{\text{ex}}(r)(\sigma_+^1 \otimes \sigma_-^2 + \sigma_-^1 \otimes \sigma_+^2), \tag{S17}$$

with $\tilde{V}_{\text{ex}}(r) = C_3/r^3$ and $r = |r|$ being the distance between the ions. The corresponding eigenstates are $|nSnS\rangle$, $|-\rangle = (|nSnP\rangle - |nPnS\rangle)/\sqrt{2}$, $|+\rangle = (|nSnP\rangle + |nPnS\rangle)/\sqrt{2}$, $|nPnP\rangle$. In particular, the eigenvalues $E_\pm(r)$ associated with $|-\rangle$ and $|+\rangle$ are shown in Fig. S1 (dashed lines). Note that $E_+(r) > E_-(r)$, $\forall r$.

We now consider the following MW dressing scheme. First, we add a bichromatic MW field coupling the state $|nP\rangle$ to another state $|n'S\rangle$, with $n' \neq n$, by a two-photon transition. The two frequencies of the bichromatic field are chosen so that they have opposite and symmetric detuning with respect to the $|nP\rangle$ to $|n'S\rangle$ transition. Thus, the bichromatic MW field causes no shift to the $|nP\rangle$ level of a single ion. However, in the presence of interactions between the $|nP\rangle$ and $|n'S\rangle$ states of a two-ion system, the pair state $|nPn'S\rangle + |n'SnP\rangle$ is shifted. As a consequence, the bichromatic MW field is no longer symmetrically detuned with respect to the transition from $|nPnP\rangle$ to $|nPn'S\rangle + |n'SnP\rangle$ and causes a shift of these two levels. In our two-state description, this energy shift can be effectively modeled by adding a contribution $\delta\mathcal{V}_{\text{PP}} = \delta E_{\text{PP}}\,|nPnP\rangle\langle nPnP|$ to the two-ion Hamiltonian.

Next, we add another red-detuned MW field coupling single-ion $|nS\rangle$ and $|nP\rangle$ states with Rabi frequency Ω_{MW} and detuning Δ_{MW}. The single-ion Hamiltonian is

$$H_{\text{MW}} = \frac{1}{2}\begin{pmatrix} \Delta_{\text{MW}} & \Omega_{\text{MW}} \\ \Omega_{\text{MW}} & -\Delta_{\text{MW}} \end{pmatrix}. \tag{S18}$$

The overall Hamiltonian for the two-ion system thus reads

$$H_{\text{ex}} = H_{\text{MW}}^{(1)} \otimes \mathbb{I}_2 + \mathbb{I}_2 \otimes H_{\text{MW}}^{(2)} + \mathcal{V}_{\text{ex}} + \delta\mathcal{V}_{\text{PP}}, \tag{S19}$$

with $\mathbb{I}_2$ the 2×2 identity matrix. The red-detuned MW field couples the $|nSnS\rangle$ and $|+\rangle$ states. Since $|nPnP\rangle$ is far detuned (due to the presence of the bichromatic MW field), this coupling results in a shift of the $|+\rangle$ state. On the contrary, $|-\rangle$ is not coupled to any state by the red-detuned MW field and does not experience any shift. In particular, when $\Delta < 0$, the energy of $|+\rangle$ is lowered in a such a way that $E_+(r)$ and $E_-(r)$ cross at a given ion-ion distance r^* [see solid curves in Fig. S1(a)]. The effective two-ion exchange potential $V_{\text{ex}}(r)$ is readily obtained by subtracting $E_+(r)$ and $E_-(r)$ and it is shown in Fig. S1(b). Clearly, $V_{\text{ex}}(r^*) = 0$, with r^* denoted by the vertical dashed line in panels (b) and (c). By properly tuning Ω_{MW} and Δ_{MW} it possible to make r^* coinciding with the distance r^0 between the ions in their equilibrium positions (see main text). In particular,
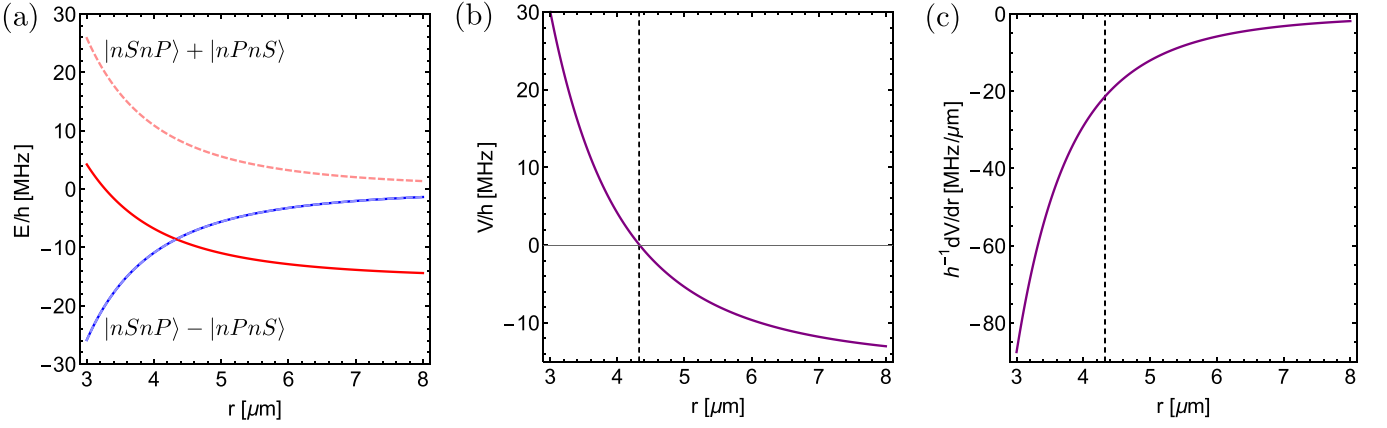
FIG. S1. **MW dressed potential.** (a) Eigenvalues of $\mathcal{V}_{\text{ex}}$, $E_-(r)$ (dashed light blue) and E_+ (dashed light red) (corresponding to the states $|-\rangle$ and $|+\rangle$), as a function of the ion-ion distance r. A bichromatic MW field shifts the energy of the $|nPnP\rangle$ state by $\delta E_{\text{PP}} = 2\pi \times 697.94$ MHz (not shown). In the presence of second red-detuned MW field with Rabi frequency $\Omega_{\text{MW}} = 2\pi \times 43$ MHz and detuning $\Delta_{\text{MW}} = -2\pi \times 50$ MHz, the energy of the bare eigenvalue $E_+(r)$ is lowered (solid red), while the one of $E_-(r)$ is unchanged (solid blue). (b) Effective exchange interaction potential $V_{\text{ex}}(r)$ as a function of the ion-ion distance r, obtained by subtracting the shifted values of $E_+(r)$ and $E_-(r)$ given by the solid curves of panel (a). (c) Gradient $|\nabla_r V_{\text{ex}}(r)|$ as a function of r. In panels (b) and (c), the vertical dashed line corresponds to $r = 4.3$ μm $\approx r^0$, where $V_{\text{ex}}(r^0) = 0$ and $|\nabla_r V_{\text{ex}}(r)|_{r=r^0} \neq 0$. In all panels, $n = 50$ and $C_3 = 697.94$ MHz μm^3.

from Fig. S1(c), one can see that this dressing scheme allows us to obtain a gradient $|F(r^0)| = |\nabla_r V_{\text{ex}}(r)|_{r=r^0}$ of the order of $2\pi \times 20$ MHz/μm, as the one we employed in the main text.

Note that the potential $V_{\text{ex}}(r)$ shown in Fig. S1(b) does not vanish at infinity distance, as it should. The reason of this fact is that, in our model, we assumed that the effect of the bichromatic MW field is to induce a large shift in the energy of the $|nPnP\rangle$ state. As a consequence, since $|nPnP\rangle$ is out of resonance, the second red-detuned MW field of Eq. (S19) only couples $|nSnS\rangle$ to $|+\rangle$, allowing us to realize the crossing between $E_+(r)$ and $E_-(r)$ shown in Fig. S1(a). However, the assumption that the $|nPnP\rangle$ level is shifted away from the other states by a significant amount of energy relies on the fact that the bichromatic MW coupling strength between $|n'Sn'S\rangle$ and $|nPnP\rangle$ is not zero which, in turn, requires a finite interaction between the $|n'S\rangle$ and $|nP\rangle$ Rydberg states. This condition can only be satisfied at finite distances. Therefore, in the long distance limit, the shift of the $|nPnP\rangle$ state (and, consequently, the one of $|+\rangle$) will vanish in such a way that $V_{\text{ex}}(r) \to 0$ for $r \to \infty$.

BORN-OPPENEHIMER APPROXIMATION WITH THE DIAGONAL CORRECTION

Finally, in this section we briefly comment about the Born-Oppenheimer (BO) approximation we used in the main text and, in particular, on the inclusion of the diagonal BO correction (DBOC). First, we write the total wavefunction of the system in the adiabatic representation [19, 31],

$$|\Psi(\boldsymbol{q}, t)\rangle = \sum_{\mu=\pm} \tilde{\phi}_\mu(\boldsymbol{q}, t) |\varphi_\mu(\boldsymbol{q})\rangle, \qquad (S20)$$

where $|\varphi_\mu(\boldsymbol{q})\rangle$ are the eigenstates of the spin Hamiltonian H_{spin} and are given in Eq. (8) of the main text, while $\tilde{\phi}_\mu(\boldsymbol{q}, t)$ are the nuclear wavefunction components. The time evolution of $|\Psi(\boldsymbol{q}, t)\rangle$ is governed by the Schrödinger equation $i\partial_t |\Psi(\boldsymbol{q}, t)\rangle = H |\Psi(\boldsymbol{q}, t)\rangle$, with H the full system Hamiltonian defined in Eq. (1) of the main text. Substituting in the latter the adiabatic representation given in Eq. (S20), we obtain the following coupled equations governing the evolution of the adiabatic components of the nuclear wavefunction $\tilde{\phi}_\mu(\boldsymbol{q}, t)$ [30],

$$i\partial_t \tilde{\phi}_\mu(\boldsymbol{q}, t) = \left[-\frac{\nabla_{\boldsymbol{q}}}{m} + V_\mu(\boldsymbol{q}) \right] \tilde{\phi}_\mu(\boldsymbol{q}, t) + \sum_\nu D_{\mu\nu}(\boldsymbol{q}) \tilde{\phi}_\nu(\boldsymbol{q}, t), \qquad (S21)$$

where the non-adiabatic couplings are defined as

$$D_{\mu\nu}(\boldsymbol{q}) = -\frac{1}{m} \left[\langle \varphi_\mu(\boldsymbol{q}) | \nabla_{\boldsymbol{q}}^2 | \varphi_\nu(\boldsymbol{q}) \rangle + 2 \langle \varphi_\mu(\boldsymbol{q}) | \nabla_{\boldsymbol{q}} | \varphi_\nu(\boldsymbol{q}) \rangle \cdot \nabla_{\boldsymbol{q}} \right]. \qquad (S22)$$
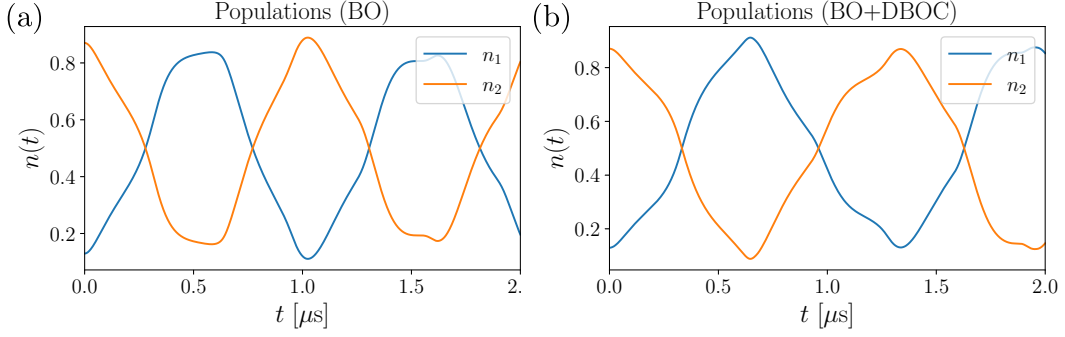
FIG. S2. **Dynamics of the diabatic population in the BO and BO+DBOC approximation.** Time evolution of the populations $n_k(t)$ of the diabatic states $|\pi_1\rangle$ (blue curve) and $|\pi_2\rangle$ (yellow curve) in the (a) BO approximation [same as Fig. 3(a) of the main text] and (b) BO+DBOC approximation with $V^0_{ex} = 0$. (b) Despite the presence of the addition potential energy contribution due to the DBOC, the diabatic populations still oscillate and swap with each other. The only difference with respect to the BO approximation of panel (a) is that the period of the oscillations is slightly increased. The system is initialized on the lower PES in the state $|\psi_0(\boldsymbol{q})\rangle$ (see main text), with $X^0_{ss} = -0.024$ μm, $Z^0_{ss} = 0$ μm, $x^0_{ss} = -0.011$ μm, and $z^0_{ss} = 4.31$ μm. Other parameters are as in Fig. 2 of the main text.

In the BO approximation the last term in Eq. (S21) is neglected and the dynamics of the nuclear wavefunctions on the two potential energy surfaces (PESs) are decoupled. Focusing on the case with $V^0_{ex} = 0$, the DBOCs are given by the diagonal elements of the non-adiabatic coupling matrix [19, 52],

$$D_{\mu\mu}(\boldsymbol{q}) = -\frac{1}{m}\left\langle \varphi_\mu(\boldsymbol{q})|\nabla^2_{\boldsymbol{q}}|\varphi_\mu(\boldsymbol{q})\right\rangle = -[\nabla_{\boldsymbol{q}}\Lambda(\boldsymbol{q})]^2 = \frac{1}{4m}\frac{q_x^2 + q_z^2}{(\gamma q_x^2 + \gamma^{-1}q_z^2)^2}, \tag{S23}$$

where we used Eq. (8) of the main text and defined $\gamma = \alpha^2\rho_- X^0/F_z(\boldsymbol{r}^0)$. In the presence of the DBOC, the motions of the two adiabatic components of the nuclear wavefunction $\tilde{\phi}_\mu(\boldsymbol{q}, t)$ are still decoupled but now they take place on the modified PESs $\tilde{V}_\mu(\boldsymbol{q}) = V_\mu(\boldsymbol{q}) + D_{\mu\mu}(\boldsymbol{q})$. Note that $D_{\mu\mu}(\boldsymbol{q}) \to \infty$ for $\boldsymbol{q} \to \boldsymbol{q}^* = \boldsymbol{0}$: the DBOC introduces an additional effective repulsive potential that takes into account the divergence of the non-adiabatic couplings at the CI. It is well-established that the DBOC overestimates the potential energy contribution due to the CI which, in general, is compensated by geometric phase (GP) effects [19, 52]. Thus, studying the system dynamics in the BO+DBOC approximation represents a "worst" case scenario and it allows us to assess whether the localization effect we observed in the system exact dynamics is due to the additional repulsive potential arising at the CI or to purely GP effects. By comparing the time evolution of the diabatic populations $n_k(t)$ in the BO and BO+DBOC approximations in Fig. S2, one can notice that the only effect of the additional potential barrier introduced by the DBOC is to increase slightly the period of the oscillations. This, indeed, confirms that the localization of the nuclear wavepacket is entirely due to the GP.